Research Article | Vol. 27, No. 16 | 5 Aug 2019 | OPTICS EXPRESS 22753
Optics EXPRESS

Plasmonic directional couplers using channel waveguides in random arrays of metal nanoparticles

C. E. GARCIA-ORTIZ,[1,*] V. COELLO,[1] E. PISANO,[1,2] Y. CHEN,[3] AND S. I. BOZHEVOLNYI[3]

[1]*CICESE, Unidad Monterrey, Alianza Centro 504, Apodaca, NL, 66629, Mexico*
[2]*Cátedras Conacyt - Centro de Investigaciones en Óptica, Alianza Centro 504, Apodaca, NL, 66629, Mexico*
[3]*Centre for Nano Optics, University of Southern Denmark, Campusvej 55, DK-5230 Odense M, Denmark*
**cegarcia@cicese.mx*

Abstract: Plasmonic directional couplers based on channel waveguides embedded in random arrays of metal nanoparticles (NPs) operating in near-infrared are fabricated using electron-beam lithography and investigated experimentally characterizing their performance with leakage-radiation microscopy. The power exchange between coupled waveguides, its spatial period and efficiency, along with the overall power transmission, are determined in the wavelength range from 700 to 800 nm. We introduce a simple coupled-mode approach based on three coupled waveguides. The composite system considers a waveguide consisting of NP-filled stripe with characteristics distinctly different from those of the channel waveguides. Using this model, we describe the performance of investigated composite plasmonic configurations and obtain good qualitative agreement with experimental observations.

1. Introduction

Plasmon-based photonic, or simply plasmonic devices represent, in general, nano-optical components that are designed to generate and detect, guide and control surface plasmon-polariton (SPP) modes. The intrinsic characteristic of SPP modes to be confined in subwavelength volumes persists to be one of the main motivations for their study [1]. A substantial amount of plasmonic devices, with many diverse functions and geometries, have been proposed, designed, and characterized in the past decade. Dielectric-loaded waveguides [2,3], channel and slot waveguides [4,5], nano-lenses [6,7], antennas [8,9], and plasmonic metamaterial components [10], are just a few examples of a long list of recently developed plasmonic devices with different purposes, which include multiplexing [11], beam splitting [12], filtering [13], nano-focusing [7], and directional coupling [14], among others.

Optical directional couplers (ODCs) consist of two or more closely-located optical waveguides, whose modes can couple evanescently and thereby exchange their powers, realizing, under certain conditions, complete power transfer between waveguides [15]. In general, ODCs with weakly-coupled waveguides can equivalently be viewed as independent waveguides with mode power exchange due to their coupling or as a single composite (multimode) waveguide structure, in which the power distribution across the structure varies with the propagation due to the mode interference [15,16]. Plasmonic directional couplers (PDCs) have also been explored in several configurations based on different coupling schemes and functions. Efficient power transfer and switching has been demonstrated in PDCs based on long-range plasmonic waveguides at telecom wavelengths [17–20], hybrid waveguide systems [21], slot metal-insulator-metal waveguides [22], and dielectric-loaded waveguides [23].

#367360 https://doi.org/10.1364/OE.27.022753
Journal © 2019 Received 13 May 2019; revised 11 Jul 2019; accepted 17 Jul 2019; published 25 Jul 2019

Optics EXPRESS

In this work, we consider a completely new alternative for the PDC design, which is based on two channel waveguides embedded in random arrays of metal nanoparticles (NPs) separated by a stripe filled also with NPs. The proof of concept for this type of waveguides was investigated in the previous work with straight waveguides, bends and splitters being designed and experimentally characterized [24]. The fundamental idea behind such structures is that the NP-free channels support plasmonic guided modes, while the SPP propagation through random and strongly interacting NPs is prohibited due to the SPP elastic multiple scattering resulting in the SPP localization [25–28]. In a recent study, the effect of multiple scattering of SPPs produced by random arrays of NPs has demonstrated to be able to maximize the deliverable number of input-to-output plasmonic channels for improved performance in optoelectronic devices by exploiting the decorrelation of SPP modes [29]. In the configuration presented here, the occurrence of coupling between two NP-free channels implies SPP transmission through the stripe of randomly positioned NPs. Surprisingly, the interpretation of experimental observations led us to assume that the NP stripe acts as a third waveguide that mediates the coupling between SPP modes supported by NP-free channels. Using a simple coupled-mode approach based on three coupled waveguides, we describe the performance of investigated composite plasmonic configurations obtaining good qualitative agreement with the experimental observations.

2. Materials and methods

The structures were fabricated using standard electron-beam lithography (EBL) and lift-off patterning. First, a 70-nm-thick gold film was deposited on top of a 0.17-mm-thick silica substrate. The lithographic mask consisted of a thin film of polymethyl-methacrylate (PMMA) spin-coated over the gold film, which acted as a positive resist. Then, the sample was patterned using the EBL process for subsequent development. A second evaporation process was performed to fabricate the cylindrical gold NPs, to finally remove the mask, and thus completing the lift-off process.

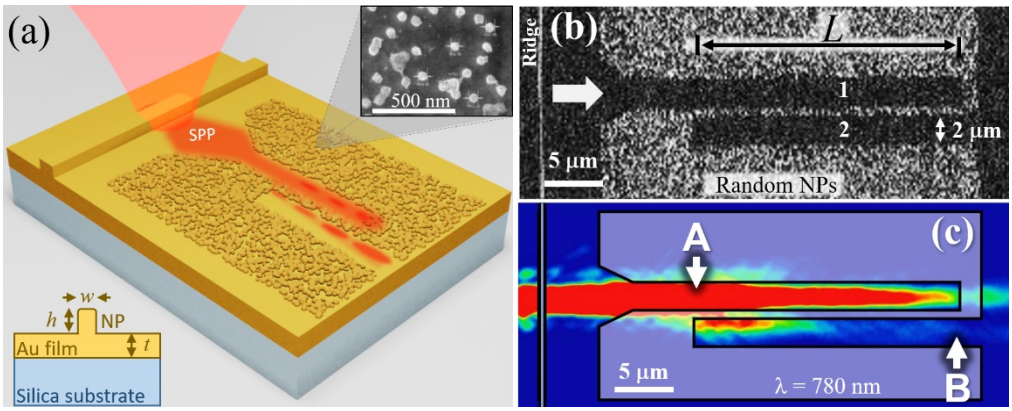

Fig. 1. (a) Schematic design of the plasmonic directional coupler and (b) scanning electron microscopy (SEM) image showing the principal waveguide (1) and the coupling channel, or adjacent waveguide (2) surrounded by the random array of metallic nanoparticles (NPs). The interaction length is denoted here as L. The inset in (a) corresponds to an SEM amplification image that shows the individual NPs which constitute the array. (c) Saturated leakage radiation microscopy image of a plasmonic directional coupler with L = 18 μm illuminated at a wavelength λ_0 = 780 nm. The position of the input and output ports (A and B) are indicated with white arrows.

The PDCs consisted of a pair of 2-μm-wide NP-free channel waveguides enclosed by a relatively high-density array of gold NPs (~75 per square micron). The design height and width of the NPs was set to h = 70 nm, and w = 50 nm, respectively. The particles were randomly distributed over the designed areas on top of the gold film [Figs. 1(a) and 1(b)]. The

Optics EXPRESS

PDCs are composed of two parallel waveguides separated by a 500-nm-wide stripe filled with NPs. It is important to mention that the ND-filled stripe has also a random distribution and that it serves as the coupling mechanism for this specific device. The separation distance between the two plasmonic waveguides was chosen following the experimental characterization conducted for different widths of the NP-filled stripe [see Appendix A]. The best coupling occurred for a separation distance of 500 nm. The interaction length L of the PDCs consists of the longitudinal distance where the two waveguides are in close proximity to each other, and where the power transfer takes place. The fabricated structures had L varied from 12 to 18 μm. The excitation of SPPs was performed using single metallic (gold) ridge, placed at 5 μm from the PDC; where a tapered channel was added to reduce the coupling losses [Fig. 1(b)].

The characterization of the samples was performed using leakage-radiation microscopy (LRM) and postprocessing image analysis in the wavelength interval from 700 to 800 nm. The basic setup and principle of operation of the LRM setup can be found in [30]. Our light source consisted of a tunable continuous-wave Ti:Saphire laser (SpectraPhysics 3900S), where the laser beam was linearly polarized and focused onto the sample using a 20x objective. The leakage radiation was collected using a 63x oil-immersion objective, which has a numerical aperture NA = 1.25; sufficient to collect the leakage radiation of the SPP modes propagating at a gold-air interface. The power distribution of the SPPs was monitored using a charge-coupled device (CCD) camera in the image plane of the microscope, and the intensity profiles were extracted from the captured digital images.

While we observed clear signs of power redistribution along the propagation, and the coupling region was clearly long enough to sustain power transfer oscillations, the power transfer was never complete [Fig. 1(c)]. Looking for the simplest approach to model this (unexpected) feature, we realized that one should either assume one of the two following possibilities: (1) that the two coupled waveguides (nominally of the same width) have very different propagation characteristics destroying the phase-matching of coupled SPP modes, or (2), considering the NP stripe as a third waveguide (with characteristics distinctly different from those of the channel waveguides) mediating the coupling between SPP modes supported by NP-free channels. The latter seems better fitting to the expectations and experimental observations

3. Three-waveguide directional-coupler model

The coupling arrangement investigated in this work was thereby considered using a three-waveguide coupled-mode approach with the PDC fields being represented by normal modes of three individual waveguides that are coupled with each other [Fig. 2(a)]. The coupled differential equations can be expressed in a matrix form as follows:

$$\frac{d}{dz}\begin{bmatrix} A_1(z) \\ A_2(z) \\ A_3(z) \end{bmatrix} = -i\begin{bmatrix} \beta_1 & \kappa_{12} & \kappa_{13} \\ \kappa_{21} & \beta_2 & \kappa_{23} \\ \kappa_{31} & \kappa_{32} & \beta_3 \end{bmatrix}\begin{bmatrix} A_1(z) \\ A_2(z) \\ A_3(z) \end{bmatrix}. \quad (1)$$

The field distributions of the j-th waveguide are denoted here as $A_j(z)$, as well as the corresponding wavevectors β_j (j = 1, 2, 3), where z is the propagation direction. The interaction between the waveguides is determined by the coupling coefficients κ_{jk} ($j \neq$ k = 1, 2, 3), which describe strength of the coupling from the j-th to the k-th waveguide. For most symmetrical systems, $\kappa_{jk} = \kappa_{kj}$, therefore we used such criterion for this model. Waveguides 1 and 3 are treated as the direct and the adjacent channel waveguides, respectively, and their wavevectors are assumed to be equal ($\beta_1 = \beta_3 = \beta_c$), since the geometrical parameters are, at some extent due to the randomness, the same. Waveguide 2 corresponds to the array of random NPs between the channels ($\beta_2 = \beta_r$). The degrees of freedom associated to the coupling coefficients was decreased by assuming that the coupling from the channel modes to

Optics EXPRESS

the random NPs mode is symmetrical and isotropic ($\kappa_{12} = \kappa_{21} = \kappa_{23} = \kappa_{32} = \kappa_r$), and that the coupling between the channel waveguides is also symmetric ($\kappa_{13} = \kappa_{31} = \kappa_c$). Equation (1) can be rewritten with the former assumptions and notations to appear as follows:

$$\frac{d}{dz}\begin{bmatrix} A_{c1}(z) \\ A_r(z) \\ A_{c2}(z) \end{bmatrix} = -i\begin{bmatrix} \beta_c & \kappa_r & \kappa_c \\ \kappa_r & \beta_r & \kappa_r \\ \kappa_c & \kappa_r & \beta_c \end{bmatrix}\begin{bmatrix} A_{c1}(z) \\ A_r(z) \\ A_{c2}(z) \end{bmatrix}. \quad (2)$$

The system of differential equations [Eq. (2)] can be solved by using a method based on finding the eigenvalues of the 3 × 3 matrix, where the three eigenvalues correspond to the propagation constants of the normal modes, and where $A_{c1}(0)$, $A_r(0)$, and $A_{c2}(0)$ are the initial conditions. A very detailed guide for solving this type of differential equations can be found in [15]. For simplicity, the mode effective indices $n_c = \beta_c/k_0$ and $n_r = \beta_r/k_0$ will be used here, where $k_0 = 2\pi/\lambda_0$ is the free-space wave vector, and λ_0 is the excitation wavelength.

We tested the model using known parameters obtained from this and previous works [Figs. 2(b)–2(g)]. The effective index of the plasmonic channel mode $n_c = (1.03 - 0.007i)$ was obtained from [24], whereas the indices of the array of gold metal NPs was varied from $n_r = 1.09$ to 1.12, based on the experimental results presented here and from [31], for the wavelength interval from 800 to 700 nm. The coupling coefficients $\kappa_r = 0.06$, and $\kappa_c = 0.03$, as well as the initial conditions $A_{c1} = 0.9$, $A_r = 0.3$, and $A_{c2} = 0$, were adjusted to match our experimental observations.

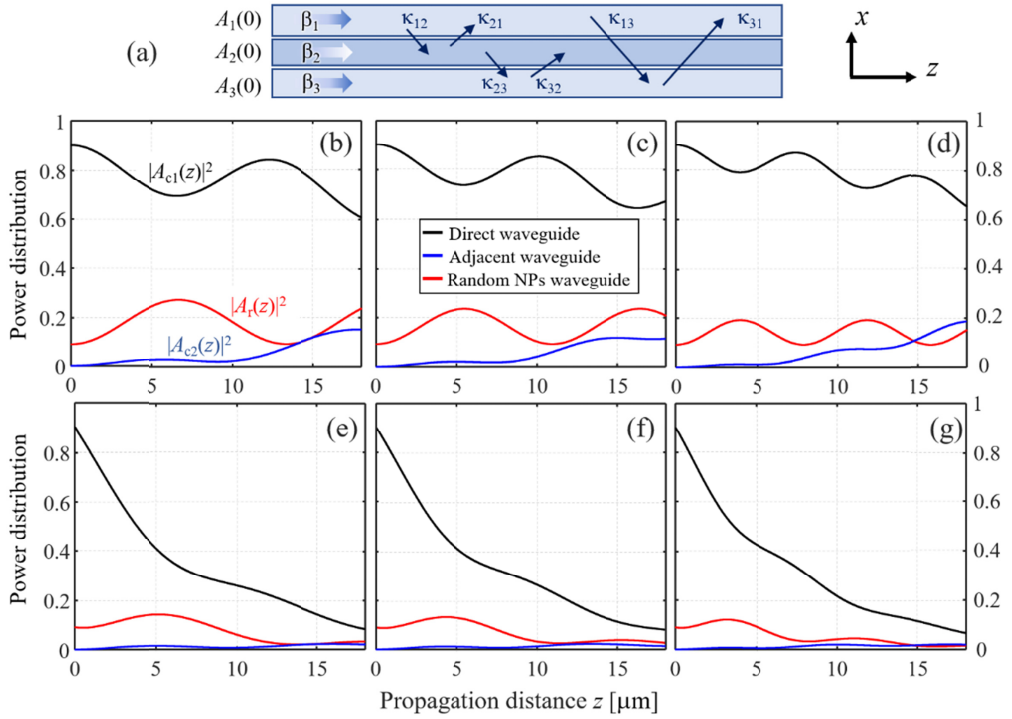

Fig. 2. (a) Schematic of the three-waveguide composite optical system. (b)–(d) Power distribution of the three waveguides along propagation (without losses) within the interaction region for different combinations of the effective indices of the random NPs waveguide and wavelengths: (b) $n_r = 1.09$, $\lambda_0 = 800$ nm; (c) $n_r = 1.10$, $\lambda_0 = 760$ nm, and (d) $n_r = 1.12$, $\lambda_0 = 700$ nm. (e)–(f) Power distributions in the three waveguides considering the propagation losses (Im[n_r] = 0.0077).

The main feature that was observed in the calculated values was the oscillating power distribution [Figs. 2(b)–2(d)]. The varying periodicity in the direct and random waveguides

Optics EXPRESS

(clearly observable in the lossless cases), is a consequence of the change of the effective-index difference $\Delta n = (n_r - n_c)$. The period shortens for larger n_r, meaning that the period decreases for shorter wavelengths. It is important to consider the three-waveguide model presented here for this composite optical system, because the coupling and waveguiding supported NP-filled stripe constitutes the principal coupling mechanism between the two main waveguides. A simpler approach, consisting of a two-waveguide model, fails to represent the system. Alternatively, a model consisting of more waveguides (or normal modes) could be, in principle, more accurate, but the high number of degrees of freedom complicates the interpretation.

4. Results and discussion

4.1 Analysis and processing of LRM images

The characterization of the PDCs starts with the visual inspection of the LRM images. First, we discuss the results obtained with the structures with L = 18 μm for the wavelength interval from 700 to 800 nm [Fig. 3]. For the shorter wavelengths, the coupled mode stays very close to the NP-filled stripe, and gradually disperses (couples) into the adjacent waveguide. At longer wavelengths, a similar trend was observed, but the mode is initially more extended into the adjacent waveguide and disperses faster. These features are explained by the fact that there is a higher confinement (larger effective index), in the stripe region, for the modes excited at shorter wavelengths and vice versa. The contrast of the images was enhanced by applying the cubic root to the intensity values obtained experimentally. The contrast-enhancement process allowed to visually observe the mode beating, which is an indication that directional coupling is taking place; although, complete power transfer was not observed. From simple inspection, it was observed that the period Π of the beating increases at longer wavelengths. In Section 4.3, a detailed analysis of the beating period is presented. Another important feature is the appearance of two maxima along the transverse coordinate x in the adjacent waveguide, which is an indication of the overlap of the normal modes of the NP-filled stripe and the channel.

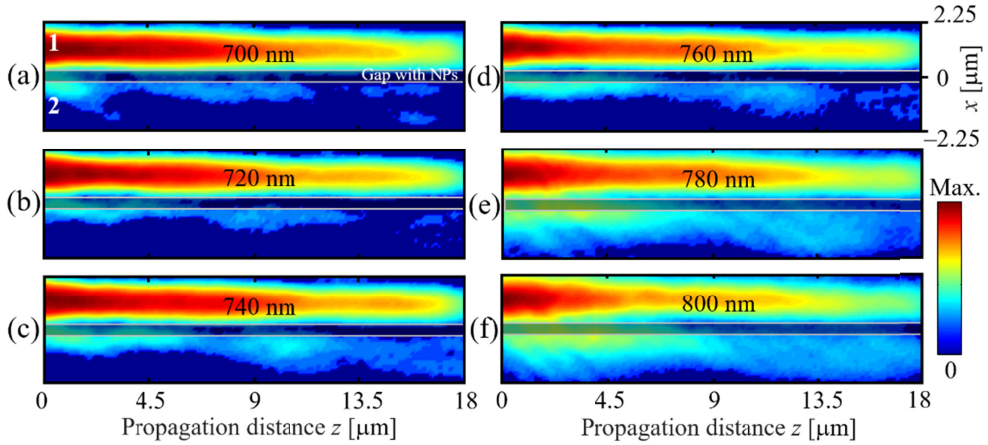

Fig. 3. Contrast-enhanced LRM images of the intensity distribution of the plasmonic modes that propagate along the direct (1) and adjacent (2) channel waveguides for the excitation wavelengths of (a) 700, (b) 720, (c) 740, (d) 760, (e) 780, and (f) 800 nm. The gray semi-transparent rectangle indicates the position of the NP-filled stripe. All images correspond to the waveguide with L = 18 μm. The contrast was enhanced by applying the cubic root to the experimental data. The color bar is not linear.

The structures with different L sizes were also explored, as all further data analysis was performed merely from the LRM images [Fig. 4]. The variation of L does not impose changes to the mode coupling in the PDC system, and the LRM images showed very similar intensity

Optics EXPRESS

distributions. Nevertheless, it was important to experimentally discard possible back reflections that could have been produced at the end of the direct waveguide. These results are used in Sections 4.2 and 4.3 to explore the transmission from point A to point B, and to provide additional images for a statistical analysis of the periodicity of the mode beating.

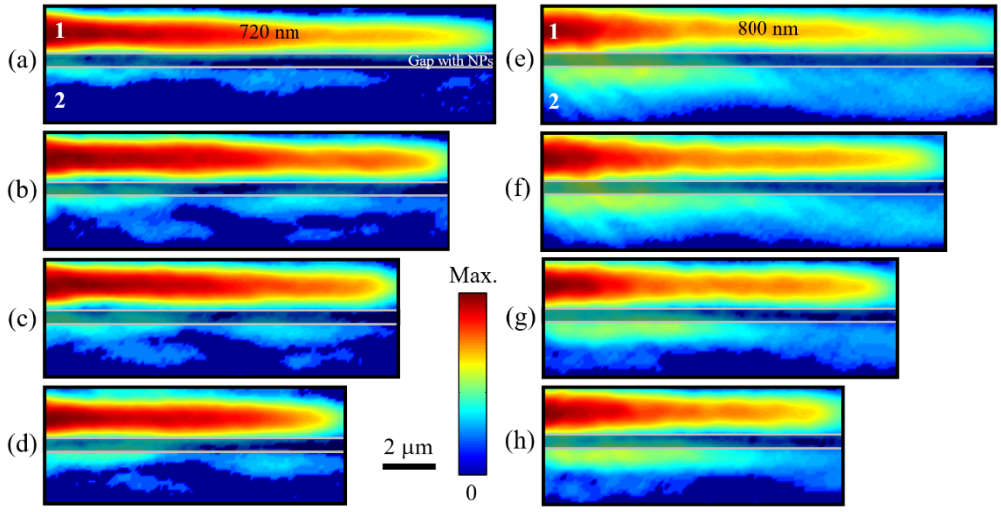

Fig. 4. Contrast-enhanced LRM images of the intensity distribution of the plasmonic modes that propagate along the direct (1) and adjacent (2) channel waveguides for the excitation wavelengths of (a)–(d) 720 nm, and (e)–(h) 800 nm. The gray semi-transparent rectangle indicates the position of the NP-filled stripe. The interaction lengths of the PDCs are 18, 16, 14, and 12 µm, from top to bottom in both columns. The contrast was enhanced by applying the cubic root to the experimental data. The color bar is not linear.

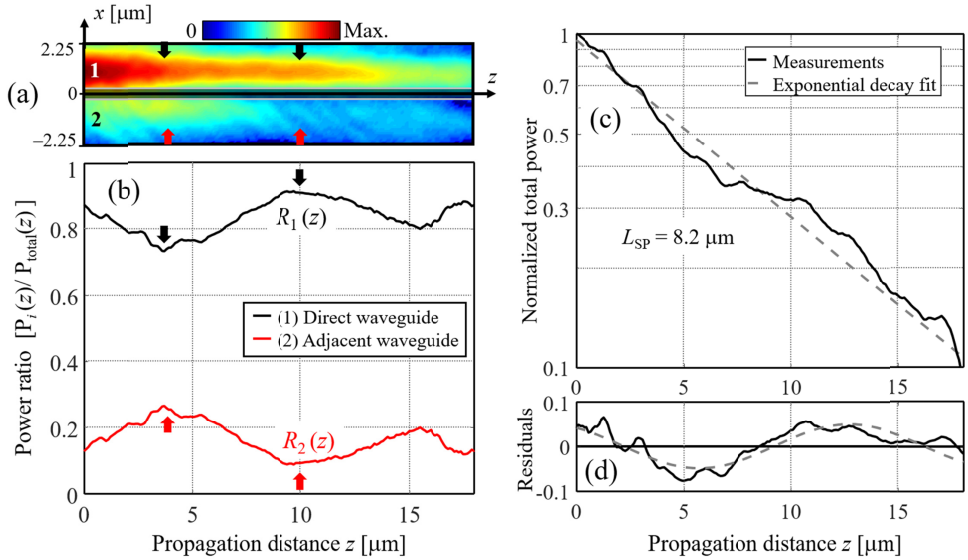

Fig. 5. (a) Contrast-enhanced LRM images of the intensity distribution in the PDC structure with L = 18 µm, excited at a wavelength λ_0 = 790 nm. The gray semi-transparent rectangle indicates the position of the NP-filled stripe. (b) Power ratio of the mode in the direct (1) and adjacent (2) waveguide to the total power, as a function of z. The arrows indicate the positions of the local maximums and minimums. (c) Normalized total power along the propagation distance, and exponential-decay fit (logarithmic scale). (d) Residuals of the measured values of the total power with respect to the exponential fit. The dashed gray line corresponds to a sinusoidal fitted curve.

Optics EXPRESS

As most plasmonic devices, the propagation losses play a significant role in the analysis of the experimental results. The propagation length L_{SP} = 8.2 μm of the PDC super-mode was estimated by integrating the intensity distribution in the transverse direction –2.25 < x < 2.25 μm of the whole structure along the propagation coordinate z [Fig. 5(a)], and fitting to an exponential-decay function [Fig. 5(b)]. This result also gives the total power $P_{total}(z)$, as a function of z, which was used to estimate the power ratios $R_i(z) = P_i(z)/P_{total}(z)$ for each of the waveguides (i = 1, 2), where P_1 corresponds to the power confined within the limits of the direct waveguide (0.25 < x < 2.25 μm), and P_2 corresponds to the power concentrated in the adjacent waveguide (–2.25 < x < –0.25 μm). Plotting the power ratios of the direct and adjacent waveguide suppresses the exponential-decay envelope, which masks the details that correspond to the coupling processes, thus easing visualization and data analysis [Fig. 5(b)]. The latter was used to get an estimation of the power transfer from the direct waveguide to the adjacent waveguide, by finding the minimum and maximum values of $R_i(z)$ [Section 4.3].

It was found that the total power $P_{total}(z)$ of the super-mode followed indeed an exponential-decay evolution (as expected), but oscillations deviating from the fit were observed [Fig. 5(c)]. Residual analysis showed that the period of the oscillations matches the period of the mode beating [Fig. 5(d)], which can be explained using the three-waveguide model explained before. The leakage-radiation microscope cannot collect the inelastic (out of plane) scattering produced by the NP-filled stripe between the channel waveguides, thus some energy will be lost as the modes propagate and couple to the stripe.

4.2 Transmission and power transfer

The transmission was measured as the ratio of the power at the output port B to the power at the input port A [Fig. 1(c)]. The power at the points A and B was determined by integrating the intensity values over an area of 2 × 2 μm^2. It was found that the transmission values increase for larger wavelengths, which, as described already, corresponds to a higher energy transfer from the direct to the adjacent waveguide. The higher transmissions (~9%) occur for the structures with shorter L (less propagation losses), and larger wavelengths (better coupling) [Fig. 6(a)]. The power transfer from the direct to the adjacent waveguide was characterized by considering the minimum value of the normalized power distribution $R_1(z)$ in the direct waveguide, and the maximum value of the $R_2(z)$ [Fig. 6(b)]. The results complement our previous observations, where it was noticed that for longer wavelengths there was a more efficient power exchange between the waveguides, with $R_1(z)$ decreasing down to 70%, and $R_2(z)$ rising up to 30%.

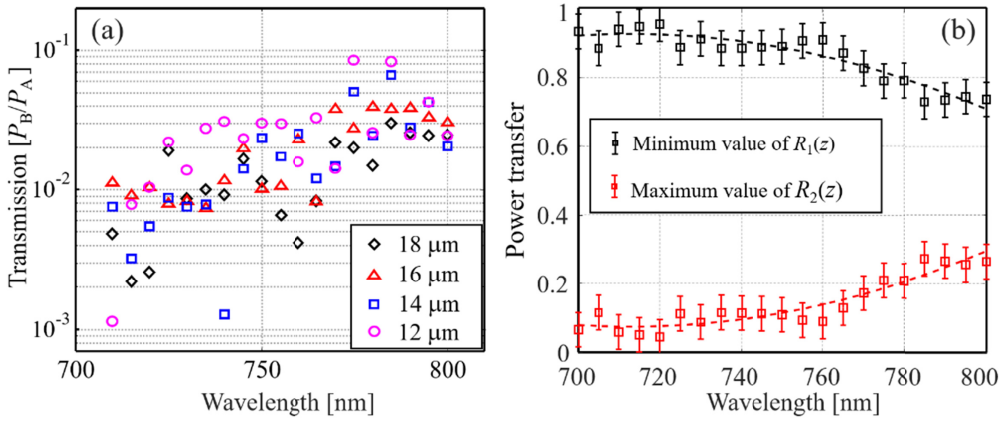

Fig. 6. (a) Power ratio of the output from the adjacent waveguide (point B) to the input of the direct waveguide (point A) as a function of wavelength, for different values of L. (b) Minimum and maximum values of $R_1(z)$ and $R_2(z)$, respectively, as a function of the wavelength for the structure with L = 18 μm. The dashed lines are a guide for the eye.

Optics EXPRESS

4.3 Beating period and effective index

The beating period Π of the power ratio distribution $R_1(z)$ was estimated by measuring and averaging the distance from peak to peak and from trough to trough [Figs. 7(a)–7(c)]. $R_1(z)$ was generally irregular, due to the randomness, so all the different possibilities to measure Π were averaged. The standard deviation was considered as the experimental uncertainty, which gave an average value of $\sigma \sim 1.5$ μm. As noted previously, the period increases slowly with the wavelength [Fig. 7(d)]. The three-waveguide model showed that Π is mainly determined by the mode effective index n_r, associated to the random array of metal NPs. The randomness of the array produces variable values for n_r, therefore, variations of Π were expected. To get an estimate of the possible values of n_r in our system, we calculated Π as a function of n_r by using the model [Fig. 7(e)]. Using the calculated values, it was possible to get a rough estimation of the dispersion of n_r, which ranged from 1.11 to 1.09, for the wavelength interval from 700 to 800 nm.

It is worth mentioning that the estimated values of n_r obtained here, are in the same range as the ones obtained experimentally in [31], where waveguides and refractive elements composed of ordered gold NPs (~100 μm^{-2}) were characterized.

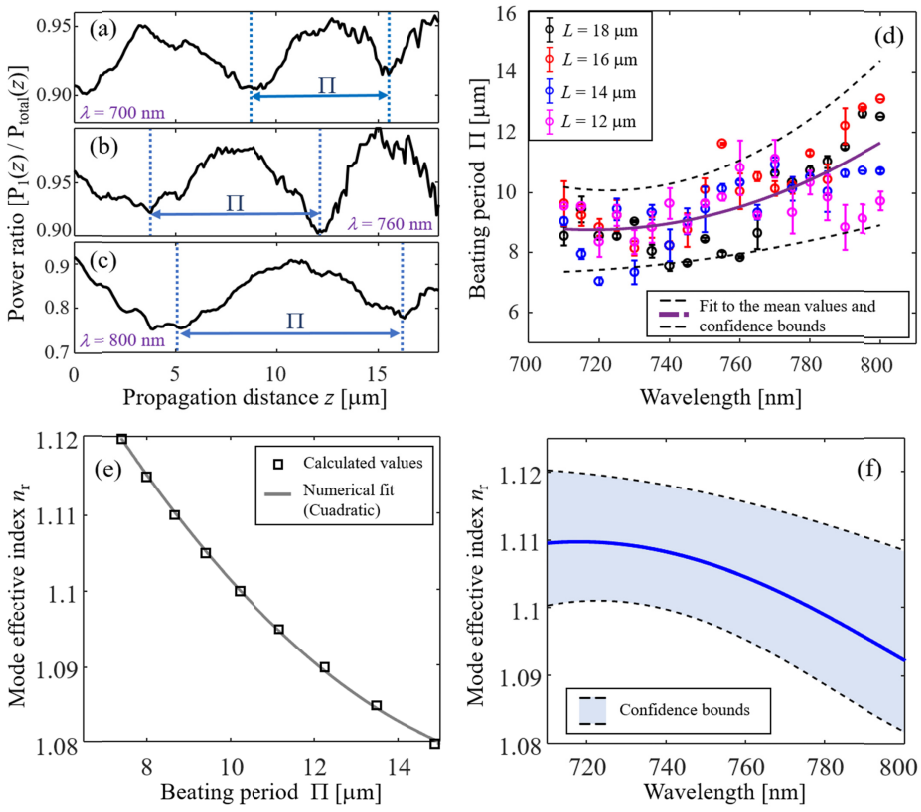

Fig. 7. (a)–(c) Power ratio of the mode in the direct waveguide with respect to the total power. The beating period Π is shown here measured from trough to trough. (d) Experimental measurements of the beating period and fit to the mean values. (e) Calculated values of Π as a function of the effective refractive index n_r of the NP-filled stripe. (f) Estimated values of n_r. The confidence bounds are associated to the experimental uncertainty of Π.

5. Conclusions

In summary, it was demonstrated that plasmonic waveguides based on NP-free channels embedded in random arrays of metallic nanoparticles can be used to realize elaborated

Optics EXPRESS

composite plasmonic nano-optical devices, such as directional couplers. The beating period, power transfer, and transmission were characterized experimentally using LRM and postprocessing image analysis. The results are in good agreement with the three-waveguide directional-coupler model that considered the NP-filled stripe as a third waveguide with characteristics distinctly different from those of the channel waveguides. This waveguide mediates the coupling between channels prohibiting at the same time a complete power transfer due to the introduced phase mismatch. The best power transfer occurred at longer wavelengths, where also the beating period and penetration increased considerably. In principle, the performance of this plasmonic device could be explored for longer excitation wavelengths, but one should bear in mind that the localization and confinement of light is strongly wavelength dependent, a circumstance that would eventually impose an upper limit on the wavelength that can still be used [25]. The three-waveguide model introduced in this work along with the estimated values of the SPP mode effective index n_r in the NP-filled stripes could be used in future to improve the performance of similar PDCs or other optoelectronic devices based on the coupling between modes guided by NP-free channels and NP-filled stripes.

Appendix A: Effect of channel separation

The width of the NP-filled stripe of metal NPs plays an important role in the process of coupling of the SPP mode from the direct waveguide to the adjacent waveguide. The width of the stripe determines also the separation between the two waveguides. An extra set of structures with different widths were fabricated to determine the effect of this parameter, where the separation distances were varied from 0.5–2.0 μm [Figs. 8(a)–8(d)]. It was found, from the LRM experimental results, that the best coupling occurred for the shortest case, which in this case corresponded to a separation distance of 500 nm.

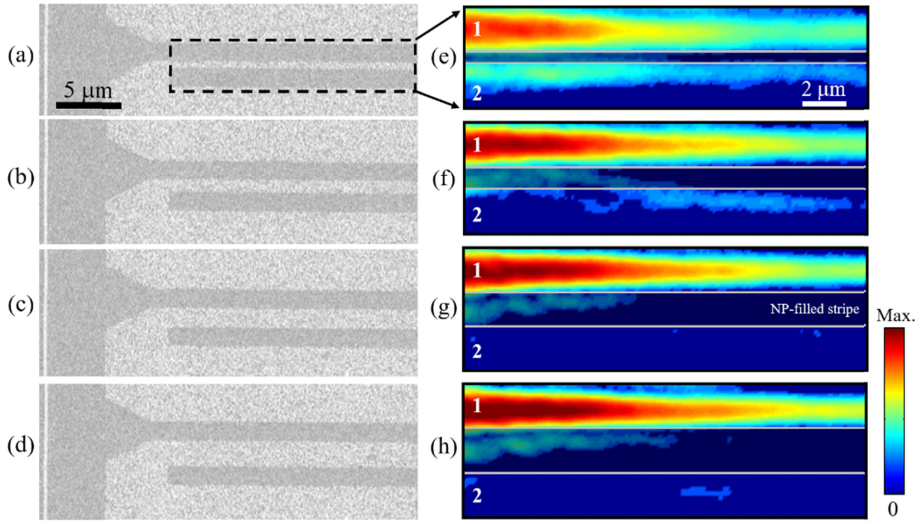

Fig. 8. (a)–(d) SEM images of the PDCs with different widths of the NP-filled stripe. The width variations were (a) 0.5, (b) 1.0, (c) 1.5 and (d) 2.0 μm. (e)–(h) Contrast-enhanced LRM images of the SPP mode in the PDCs at an excitation wavelength of 800 nm, for the different structures shown in (a)–(d).

Funding

Consejo Nacional de Ciencia y Tecnología, (250719, 252621); H2020 European Research Council; Villum Fonden.

Optics EXPRESS

Acknowledgments

C.E.G.-O. would like to thank the assistance of Abdulkareem Mas-ud and Fabiola Armenta with the image postprocessing, and insightful discussions with Dr. Ricardo Tellez-Limon on this subject.

References

1. A. Maradudin, J. R. Sambles, and W. L. Barnes, *Modern plasmonics* (Elsevier, 2014).
2. T. Holmgaard and S. I. Bozhevolnyi, "Theoretical analysis of dielectric-loaded surface plasmon-polariton waveguides," Phys. Rev. B Condens. Matter Mater. Phys. **75**(24), 245405 (2007).
3. C. Garcia, V. Coello, Z. Han, I. P. Radko, and S. I. Bozhevolnyi, "Partial loss compensation in dielectric-loaded plasmonic waveguides at near infra-red wavelengths," Opt. Express **20**(7), 7771–7776 (2012).
4. H. Okamoto, K. Kusaka, K. Yamaguchi, T. Ohtsu, M. Haraguchi, and T. Okamoto, "Self-imaging confirmed in plasmonic channel waveguides at visible wavelengths," Appl. Phys. Lett. **105**(22), 221106 (2014).
5. A. Andryieuski, V. A. Zenin, R. Malureanu, V. S. Volkov, S. I. Bozhevolnyi, and A. V. Lavrinenko, "Direct characterization of plasmonic slot waveguides and nanocouplers," Nano Lett. **14**(7), 3925–3929 (2014).
6. Z. Liu, J. M. Steele, W. Srituravanich, Y. Pikus, C. Sun, and X. Zhang, "Focusing surface plasmons with a plasmonic lens," Nano Lett. **5**(9), 1726–1729 (2005).
7. N. C. Lindquist, P. Nagpal, A. Lesuffleur, D. J. Norris, and S.-H. Oh, "Three-dimensional plasmonic nanofocusing," Nano Lett. **10**(4), 1369–1373 (2010).
8. G. Rui and Q. Zhan, "Highly sensitive beam steering with plasmonic antenna," Sci. Rep. **4**(1), 5962 (2014).
9. T. Kosako, Y. Kadoya, and H. F. Hofmann, "Directional control of light by a nano-optical Yagi–Uda antenna," Nat. Photonics **4**(5), 312–315 (2010).
10. B. J. Bohn, M. Schnell, M. A. Kats, F. Aieta, R. Hillenbrand, and F. Capasso, "Near-field imaging of phased array metasurfaces," Nano Lett. **15**(6), 3851–3858 (2015).
11. Z. Zhu, C. E. Garcia-Ortiz, Z. Han, I. P. Radko, and S. I. Bozhevolnyi, "Compact and broadband directional coupling and demultiplexing in dielectric-loaded surface plasmon polariton waveguides based on the multimode interference effect," Appl. Phys. Lett. **103**(6), 061108 (2013).
12. C. Sun, K. Rong, F. Gan, S. Chu, Q. Gong, and J. Chen, "An on-chip polarization splitter based on the radiation loss in the bending hybrid plasmonic waveguide structure," Appl. Phys. Lett. **111**(10), 101105 (2017).
13. Y. Liang, S. Zhang, X. Cao, Y. Lu, and T. Xu, "Free-standing plasmonic metal-dielectric-metal bandpass filter with high transmission efficiency," Sci. Rep. **7**(1), 4357 (2017).
14. V. A. Zenin, V. S. Volkov, Z. Han, S. I. Bozhevolnyi, E. Devaux, and T. W. Ebbesen, "Directional coupling in channel plasmon-polariton waveguides," Opt. Express **20**(6), 6124–6134 (2012).
15. C.-L. Chen, "Optical Directional Couplers and their Applications", in *Foundations for Guided-Wave Optics* (John Wiley & Sons, 2007), Chap. 6.
16. W.-P. Huang, "Coupled-mode theory for optical waveguides: an overview," J. Opt. Soc. Am. A **11**(3), 963–983 (1994).
17. T. Nikolajsen, K. Leosson, and S. I. Bozhevolnyi, "Surface plasmon polariton based modulators and switches operating at telecom wavelengths," Appl. Phys. Lett. **85**(24), 5833–5835 (2004).
18. A. Boltasseva and S. I. Bozhevolnyi, "Directional couplers using long-range surface plasmon polariton waveguides," IEEE J. Sel. Top. Quantum Electron. **12**(6), 1233–1241 (2006).
19. A. Degiron, S.-Y. Cho, T. Tyler, N. M. Jokerst, and D. R. Smith, "Directional coupling between dielectric and long-range plasmon waveguides," New J. Phys. **11**(1), 015002 (2009).
20. V. A. Zenin, V. S. Volkov, Z. Han, S. I. Bozhevolnyi, E. Devaux, and T. W. Ebbesen, "Directional coupling in channel plasmon-polariton waveguides," Opt. Express **20**(6), 6124–6134 (2012).
21. D. Zeng, L. Zhang, Q. Xiong, and J. Ma, "Directional coupler based on an elliptic cylindrical nanowire hybrid plasmonic waveguide," Appl. Opt. **57**(16), 4701–4706 (2018).
22. P. Chen, R. Liang, Q. Huang, Z. Yu, and X. Xu, "Plasmonic filters and optical directional couplers based on wide Metal-Insulator-Metal structure," Opt. Express **19**(8), 7633–7639 (2011).
23. Z. Chen, T. Holmgaard, S. I. Bozhevolnyi, A. V. Krasavin, A. V. Zayats, L. Markey, and A. Dereux, "Wavelength-selective directional coupling with dielectric-loaded plasmonic waveguides," Opt. Lett. **34**(3), 310–312 (2009).
24. E. Pisano, V. Coello, C. E. Garcia-Ortiz, Y. Chen, J. Beermann, and S. I. Bozhevolnyi, "Plasmonic channel waveguides in random arrays of metallic nanoparticles," Opt. Express **24**(15), 17080–17089 (2016).
25. S. I. Bozhevolnyi, V. S. Volkov, and K. Leosson, "Localization and waveguiding of surface plasmon polaritons in random nanostructures," Phys. Rev. Lett. **89**(18), 186801 (2002).
26. S. I. Bozhevolnyi, V. S. Volkov, K. Leosson, and A. Boltasseva, "Surface plasmon polariton waveguiding in random surface nanostructures," J. Microsc. **209**(Pt 3), 209–213 (2003).
27. S. I. Bozhevolnyi, J. Erland, K. Leosson, P. M. Skovgaard, and J. M. Hvam, "Waveguiding in surface plasmon polariton band gap structures," Phys. Rev. Lett. **86**(14), 3008–3011 (2001).
28. S. F. Liew, S. M. Popoff, A. P. Mosk, W. L. Vos, and H. Cao, "Transmission channels for light in absorbing random media: From diffusive to ballistic-like transport," Phys. Rev. B Condens. Matter Mater. Phys. **89**(22), 224202 (2014).

Optics EXPRESS

29. W. Choi, Y. Jo, J. Ahn, E. Seo, Q.-H. Park, Y. M. Jhon, and W. Choi, "Control of randomly scattered surface plasmon polaritons for multiple-input and multiple-output plasmonic switching devices," Nat. Commun. **8**(1), 14636 (2017).
30. A. Drezet, A. Hohenau, D. Koller, A. Stepanov, H. Ditlbacher, B. Steinberger, F. R. Aussenegg, A. Leitner, and J. R. Krenn, "Leakage radiation microscopy of surface plasmon polaritons," Mater. Sci. Eng. B **149**(3), 220–229 (2008).
31. I. P. Radko, A. B. Evlyukhin, A. Boltasseva, and S. I. Bozhevolnyi, "Refracting surface plasmon polaritons with nanoparticle arrays," Opt. Express **16**(6), 3924–3930 (2008).